

Article

Online Cell-by-Cell Calibration Method to Enhance the Kalman-Filter-Based State-of-Charge Estimation

Ngoc-Thao Pham , Phuong-Ha La , Sungoh Kwon  and Sung-Jin Choi * 

Department of Electrical, Electronic and Computer Engineering, University of Ulsan, Ulsan 44610, Republic of Korea; ptnthao1776@gmail.com (N.-T.P.); laphuongha@gmail.com (P.-H.L.); sungoh@ulsan.ac.kr (S.K.)

* Correspondence: sjchoi@ulsan.ac.kr

Abstract: Kalman filter (KF) is an effective way to estimate the state-of-charge (SOC), but its performance is heavily dependent on the state-space model parameters. One of the factors that causes the model parameters to change is battery aging, which is individually and non-uniformly experienced by the cells inside the battery pack. To mitigate this issue, this paper proposes an online calibration method considering the impact of cell aging and cell inconsistency. In this method, the state-of-health (SOH) levels of the individual cells are estimated using the deep learning method, and the historical parameter loop-up table is constructed to update the state-space model. The proposed calibration framework provides enhanced accuracy for cell-by-cell SOC estimation by lightweight computing devices. The SOC estimation errors of the calibrated EKF reduce to 1.81% compared to 12.1% of the uncalibrated algorithms.

Keywords: battery aging; cell inconsistency; Kalman filter; state-of-charge (SOC) estimation; state-of-health (SOH) estimation

1. Introduction



Academic Editor: Federico Baronti

Received: 24 December 2024

Revised: 24 January 2025

Accepted: 29 January 2025

Published: 2 February 2025

Citation: Pham, N.-T.; La, P.-H.; Kwon, S.; Choi, S.-J. Online Cell-by-Cell Calibration Method to Enhance the Kalman-Filter-Based State-of-Charge Estimation. *Batteries* **2025**, *11*, 58. <https://doi.org/10.3390/batteries11020058>

Copyright: © 2025 by the authors. Licensee MDPI, Basel, Switzerland. This article is an open access article distributed under the terms and conditions of the Creative Commons Attribution (CC BY) license (<https://creativecommons.org/licenses/by/4.0/>).

Recently, transportation has been rapidly electrified, aiming to reduce fossil fuel consumption by virtue of policy support from governments [1,2]. Due to the significant rise in demand, the unit price of lithium-ion batteries has been decreasing, which is accelerating the expansion of electric vehicle fleets [3]. The battery pack is the most important; thus, a reliable and effective battery management system is required [4,5]. Since the battery is sensitive to over-charging and under-discharging issues, it is essential to monitor the energy level of the battery pack to optimize the operation range of the EV [6,7]. The energy level of the battery is estimated by observing the change of voltage, current, and temperature under specific operating conditions [8–10].

To ensure safety, accurate SOC estimation is crucial. The existing battery state estimation method for the battery pack assumes that every cell inside the pack has uniform characteristics. This belief comes from the fact that the characteristics of the cells are screened before the packing process [11], and thus, the estimation algorithm is implemented just for the whole battery pack. However, it is reported that such an assumption is only valid in the early cycles of charging and discharging processes. Various reports warn that the battery characteristics of the cells are gradually changing during operation and the aging patterns of the cells are also dissimilar [12–14]. The cell inconsistency inside the battery pack can make the individual cells suffer from over-charging or under-discharging issues [15]. Consequently, cell-level state estimation is strongly demanded.

Many SOC and SOH estimation methods have been introduced in the literature [15,16]. Battery state estimation methods can be classified into three categories, including Coulomb counting, model-based estimation, and data-driven estimation. The Coulomb counting methods measure the operating current of the battery pack to calculate the amount of charge that flows into or out of the battery [17,18]. These methods are popular in industrial applications due to their simplicity, but the estimation accuracy is strongly dependent on the measurement noise. Furthermore, the initial SOC levels of the battery cells/pack have to be clearly identified, but it is quite difficult.

To overcome the limitation of the Coulomb counting methods, model-based methods such as KF or observer can be a viable alternative. From the past and present information such as voltage, current, and temperature, the SOC level is estimated accordingly [19–22]. Due to its state-space equation based on the physical model, high estimation accuracy can be achieved with low computation time. Additionally, sensing noise can be canceled and the estimation can be flexibly adapted to changes in operating conditions. However, the model-based methods require exact model parameters and the OCV-SOC relation to ensure successful estimation [23–25]. As the battery ages, the state-space model of the KF deviates from the true value, and the estimation error increases. Thus, the state-space models of the Kalman-based estimator have to be re-calibrated to account for battery degradation to ensure the estimation accuracy.

By the way, data-driven estimation methods have recently been introduced. Machine learning (ML), deep learning (DL), or artificial intelligence (AI) algorithms can quite accurately estimate the SOC or SOH levels of the battery cell/pack [26–30]. However, they require a huge dataset to train the estimation model. Thus, it takes considerable computation time. Additionally, a high-performance computing machine poses a cost burden.

Therefore, it is reasonable to think that by combining the advantages of the model-based and data-driven estimation methods, the disadvantages in terms of estimation time, accuracy, and implementation feasibility are progressively improved. The data-driven methods such as long short-term memory (LSTM), reinforcement learning, adaptive forgetting factor regression least-squares, or extreme learning machine algorithms have been utilized to tune the state-space model parameters of the Kalman-estimator [31–36]. However, these methods have not yet accounted for the impact of cell aging and inconsistency. As a result, the estimation error increases as the battery undergoes degradation.

To mitigate this limitation, this paper proposes an online calibration method that employs the DL algorithm for accurate KF estimation of individual cells. Contributions of this work are as follows:

- Impact of cell aging on the KF estimator has been investigated.
- Online calibration framework adjusting the EKF parameters dynamically has been introduced to enhance the accuracy of SOC estimation against the aging process.
- Various DL algorithms with different training dataset size have been considered for SOH estimation to optimize the proposed algorithm.

The remaining contents of this paper are as follows. The impacts of aging and cell inconsistency on the estimation accuracy are analyzed in Section 2 and the proposed algorithm is described in Section 3. The performance of the proposed method is verified in Section 4, and the conclusion is presented in Section 5.

2. Impact of Aging and Cell Inconsistency on the KF Estimator

2.1. Consideration of the Cell's Aging Effect

To assess the impact of aging on the KF estimator, the cylindrical 18,650 battery cells (3.6 V-2.9 Ah) are cycled under various test conditions. The experimental setup is illustrated

in Figure 1, where the cells are placed inside a thermal chamber. The cells are charged by the CC-CV method at 0.5 C-rate and 4.2 V, then fully discharged by the CC method at various current levels (0.5 C, 1.5 C, 2 C). To accelerate the aging mechanism, these cells are charged and discharged continuously by a cycler test system (Maccor 4300K).

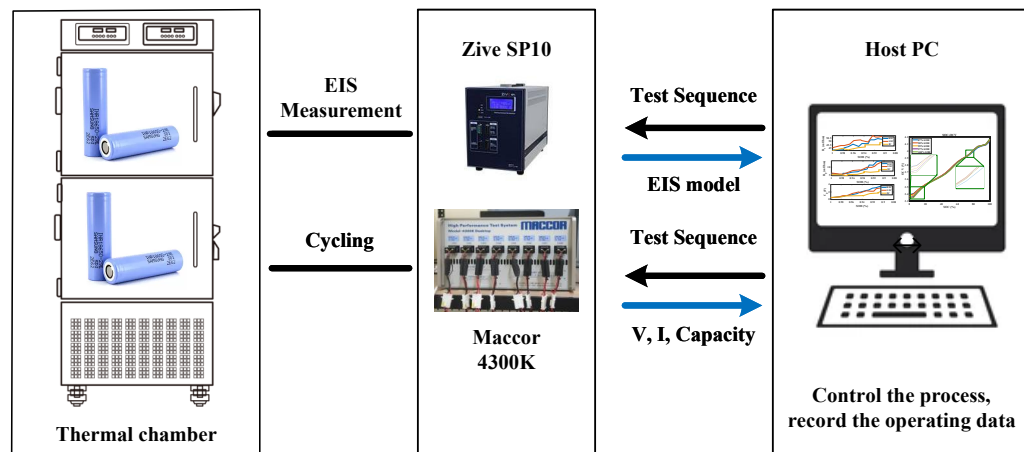


Figure 1. Experimental setup for the aging dataset.

Furthermore, the electrochemical impedance spectroscopy (EIS) models of the cells are extracted every 50 cycles of charging and discharging processes by an impedance analyzer (Zive SP10, WonATech, Seoul, Republic of Korea). This analyzer employs the sinusoidal frequency sweep method, where a sinusoidal signal is injected into the battery to observe the response signal under various frequencies. A potentiostat is applied to inject voltage with a frequency sweep from 10 kHz to 0.1 Hz. The resulting battery EIS is determined by voltage and response current. The measurement is conducted at every 5% SOC.

The host PC controls the cycling processes and records the data. In this paper, the ambient temperature inside the thermal chamber is fixed at 25 degrees Celsius. By repeating the cycling process, the aging patterns of the cells can be collected. Later, the operation information during the cycling process is used to train the DL estimator in Section 3.

After collecting, raw battery data (voltage, current, temperature, capacity, and EIS) will be processed for implementing SOC and SOH estimation. SOC is calculated as

$$SOC(t) = \frac{C_{\text{remaining}}(t)}{C_n} \times 100\%. \quad (1)$$

And SOH is defined as

$$SOH = \frac{C_n}{C_{\text{rated}}} \times 100\% \quad (2)$$

where $C_{\text{remaining}}$ is the amount of charge remaining in the cell; C_n indicates the actual full capacity of the battery at the time n ; C_{rated} is the rated battery capacity. The equivalent impedance parameters are extracted from the collected EIS data using a genetic algorithm [37].

The EIS models extracted after every 50 cycles form a historical dataset. Although the dynamic response of the cell can be presented by various EIS model types [38], the Thévenin equivalent circuit, as shown in Figure 2, is utilized in this paper due to its simplicity. Based on the recorded dataset, the cell impedance and OCV-SOC curve show a drift during the operation, as in Figure 3. The EIS model parameters (R_s , R_p , and C_p) in Figure 3a increase as the SOH decreases from 100% to 90%. On the other hand, the OCV-SOC curves also show some shift according to the SOH change, as shown in Figure 3b, which causes additional

errors in the SOC estimation. Thus, the SOC estimation should consider the aging patterns, especially for the KF estimators.

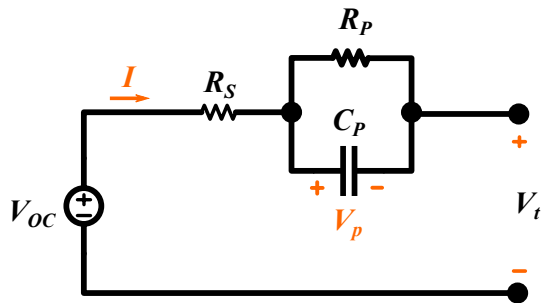


Figure 2. Thévenin model for the battery cell.

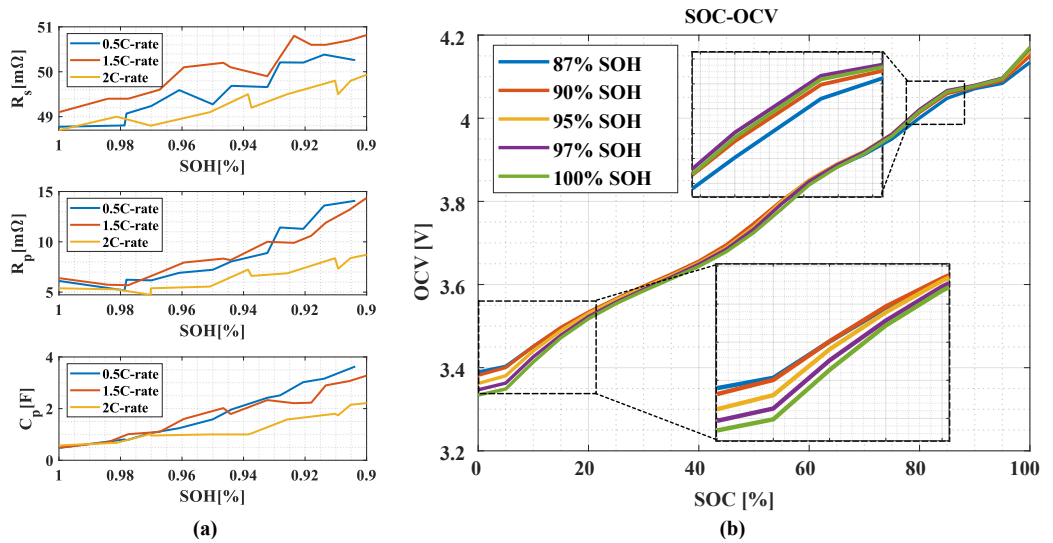


Figure 3. Impact of the aging on the EIS model: (a) model parameter change; (b) OCV-SOC curve shift.

Since the Extended Kalman Filter (EKF) estimator is the most popular method among the family of KF-estimator for battery state estimation [39], it is advisable to observe the battery aging effect in the EKF estimator. Here, the EKF formulation is described as follows. Based on the equivalent circuit in Figure 2, the charge level, SOC, polarization voltage, V_p , and the terminal voltage, V_t , of the cell at a sampling point are calculated by

$$SOC(k+1) = SOC(k) - \frac{\eta \Delta t}{C_n} i(k) \quad (3)$$

$$V_p(k+1) = V_p(k) e^{-\frac{\Delta t}{R_p C_p}} - R_p i(k) [1 - e^{-\frac{\Delta t}{R_p C_p}}] \quad (4)$$

$$V_t(k) = V_{OC}(k) - V_p(k) - i(k) R_s \quad (5)$$

where the open-circuit voltage is denoted by V_{OC} ; η is the Coulombic efficiency during the discharging and charging process; i is the discharge current of the cell; C_n is the actual full capacity of the cell at an SOH level; and Δt is the sampling time interval.

Through the linearization process, the state-space equations are formed as

$$\begin{bmatrix} SOC(k+1) \\ V_p(k+1) \end{bmatrix} = A_k \begin{bmatrix} SOC(k) \\ V_p(k) \end{bmatrix} + B_k i(k) + \omega(k) \quad (6)$$

$$V_t(k) = C_k \begin{bmatrix} SOC(k) \\ V_p(k) \end{bmatrix} + D_k i(k) + v(k) \quad (7)$$

where SOC and V_p are regarded as the state variables and V_t is the output variable. ω and v are the state process noise and measurement noise, respectively. Both are assumed to be Gaussian white noise with zero mean. The covariances of $\omega(k)$ and $v(k)$ are Q and R , respectively. A_k , B_k , C_k , and D_k are the Jacobian matrices of the EKF and are, respectively, formulated as

$$A_k = \begin{bmatrix} 1 & 0 \\ 0 & e^{-\frac{\Delta t}{R_p C_p}} \end{bmatrix}, \quad (8)$$

$$B_k = \begin{bmatrix} -\frac{\Delta t \eta}{C_n} \\ R_p \left(1 - e^{-\frac{\Delta t}{R_p C_p}} \right) \end{bmatrix}, \quad (9)$$

$$C_k = \begin{bmatrix} \frac{\delta V_{OC}}{\delta SOC} & -1 \end{bmatrix}, \quad (10)$$

$$D_k = -R_s. \quad (11)$$

where $\frac{\delta V_{OC}}{\delta SOC}$ is the derivative of the OCV with respect to SOC.

After defining the state-space equation for battery, the EKF process is implemented with two main stages as follows:

- Prediction (time update)
State estimation:

$$\hat{x}_{k+1|k} = A_{k+1} \hat{x}_{k|k} + B_{k+1} u_k \quad (12)$$

The error covariance:

$$P_{k+1|k} = A_{k+1} P_{k|k} A_{k+1}^T + Q \quad (13)$$

- Correction (measurement update)
Kalman gain:

$$K_{k+1} = P_{k+1|k} C_{k+1}^T (C_{k+1} P_{k+1|k} C_{k+1}^T + R)^{-1} \quad (14)$$

State variable:

$$\hat{x}_{k+1|k+1} = \hat{x}_{k+1|k} + K_{k+1} (z_{k+1} - C_{k+1} \hat{x}_{k+1|k}) \quad (15)$$

The error covariance:

$$P_{k+1|k+1} = (1 - K_{k+1} C_{k+1}) P_{k+1|k} \quad (16)$$

where k represents the iteration index; x is the state vector and u is the control input vector; A, B, and C are the transition matrix, input matrix, and measurement matrix, respectively; P denotes the error covariance; K indicates Kalman gain; z is the observed output vector; and subscripts |k and |k+1 denote the predicted and updated values. In this study, Q and

R are determined using a trial-and-error approach and are regarded as $Q = \begin{bmatrix} 10^{-5} & 0 \\ 0 & 10^{-4} \end{bmatrix}$, $R = 0.002$.

The EKF framework uses Jacobian matrices derived from the functions of the EIS-model parameters, actual available capacity, and OCV-SOC characteristic curve. To further verify the impact of aging on the SOC estimation error, the SOC estimation is performed both at 100% and 87% SOH level using the same state-space model, where the A_k , B_k , C_k , and D_k matrices are extracted at 100% SOH level. The SOC profile illustrated in Figure 4 indicates that the RMSE rises to 9.6% during charging and 12.1% during discharging at an 87% SOH level, compared to 1.08% and 1.79% for charge and discharge, respectively, at the 100% SOH level. Thus, it can be seen that the EKF estimators should be compensated to improve the accuracy.

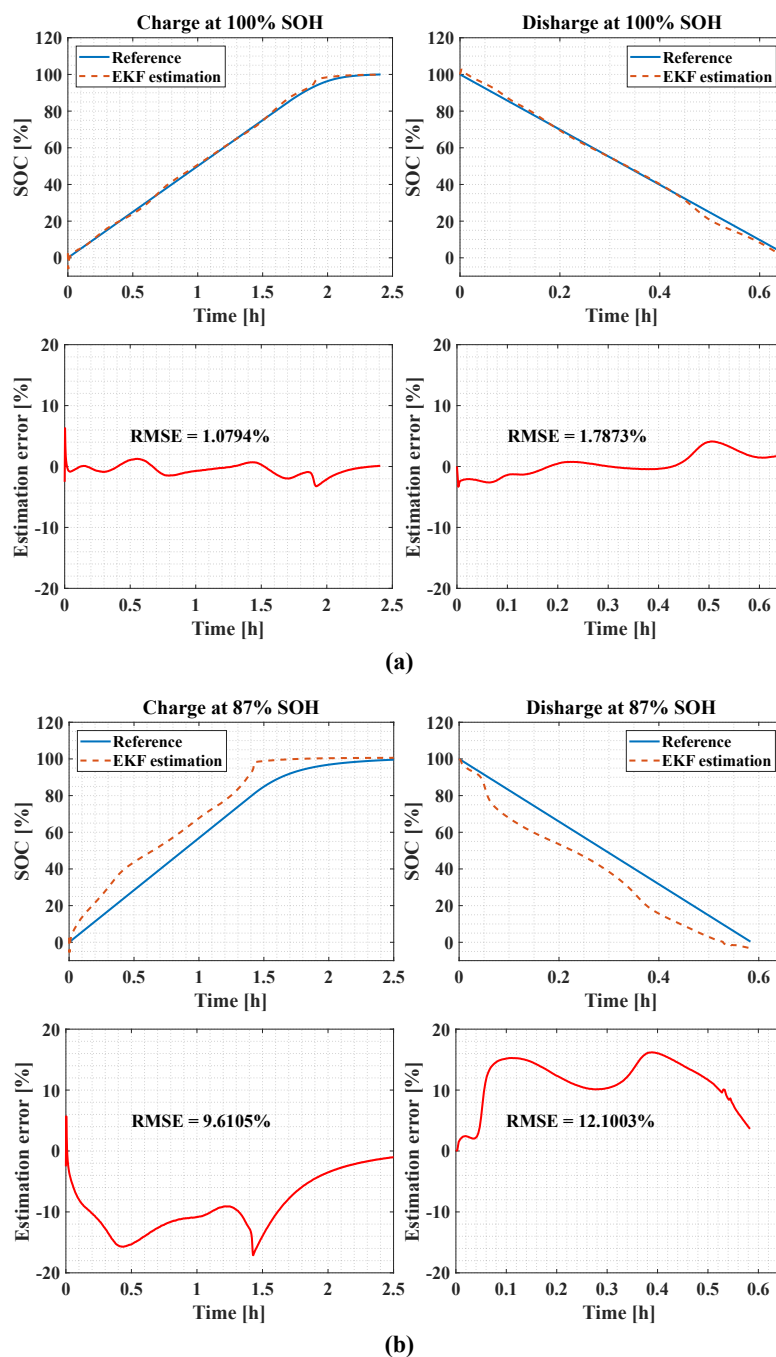


Figure 4. SOC profile and the estimation error **(a)** at 100% SOH level; **(b)** at 87% SOH level.

2.2. Consideration of the Cell Inconsistency Effect

Although individual characteristics of the cells inside the same battery pack are assembled to be maximally uniform by quality control, inherent mismatching is unavoidable due to the material and production tolerance. Additionally, the aging patterns experienced by the cells are not the same as each other. Consequently, the battery pack can lead to over-charging or under-discharging issues, as in Figure 5a. To ensure safety, the battery management system (BMS) is utilized to monitor the terminal voltage of the cells during their operation, as in Figure 5b. However, the mismatching of the EIS model parameters, available capacity, and OCV-SOC relationship creates significant challenges in safety and battery capacity utilization. As the EIS model parameters change with aging, cell inconsistency becomes more pronounced. Therefore, individual battery states, such as SOC and SOH levels, must be estimated for improved safety.

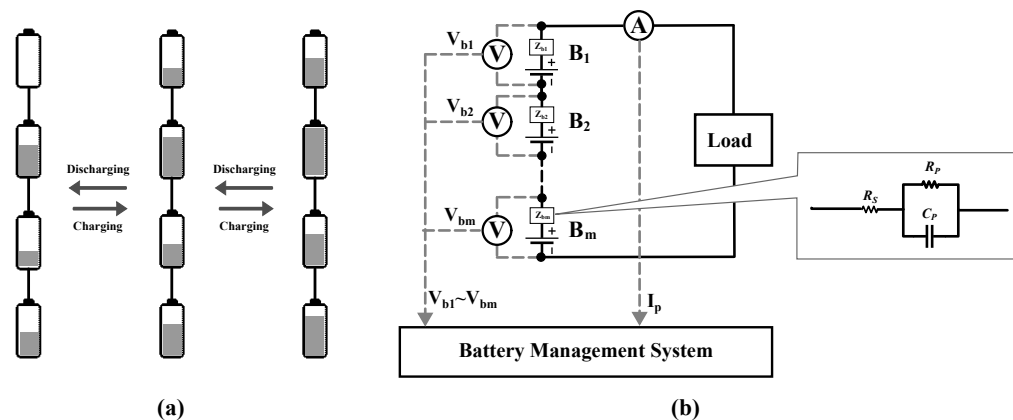


Figure 5. Cell inconsistency issue: (a) safety and capacity utilization; (b) cell monitoring by BMS.

3. Online Calibration for the KF Estimator

3.1. Proposed Calibration Framework

In order to handle the individual cell state estimation, an online estimation hardware device is added to the conventional BMS unit, as shown in Figure 6a. In this paper, NVIDIA Jetson Nano [40], which is specially designed for ML, DL, and AI purposes, is adopted. During the operation, the BMS collects cell voltages and currents and transmits them to the online estimation device, which returns the estimated SOH and SOC for the individual cells.

The flowchart for the calibration process implemented on the estimation device is illustrated in Figure 6b. When the DL SOH-estimator is executed, the actual SOH level and calibrating parameters such as actual available capacity, EIS-model, and OCV-SOC relationship are updated for KF-estimator. Such a calibration is executed for every cell in the pack. Hence, the SOC levels of every cell can be estimated with improved accuracy. Since the SOH levels are slowly changing, the calibration needs to be periodically executed over a long-term period. The updated state-space model of the KF-estimator will be retained until the new calibration parameters are updated in the next period.

By the way, the dataset for model training is only limited to a few battery cells and sometimes fails to cover the behavior of all cells. To alleviate this problem, the actual operating performance of the cells is recorded during their operation as a buffer dataset. During each periodic calibration sequence, the model is trained to adapt to each cell, further enhancing the accuracy of the estimation.

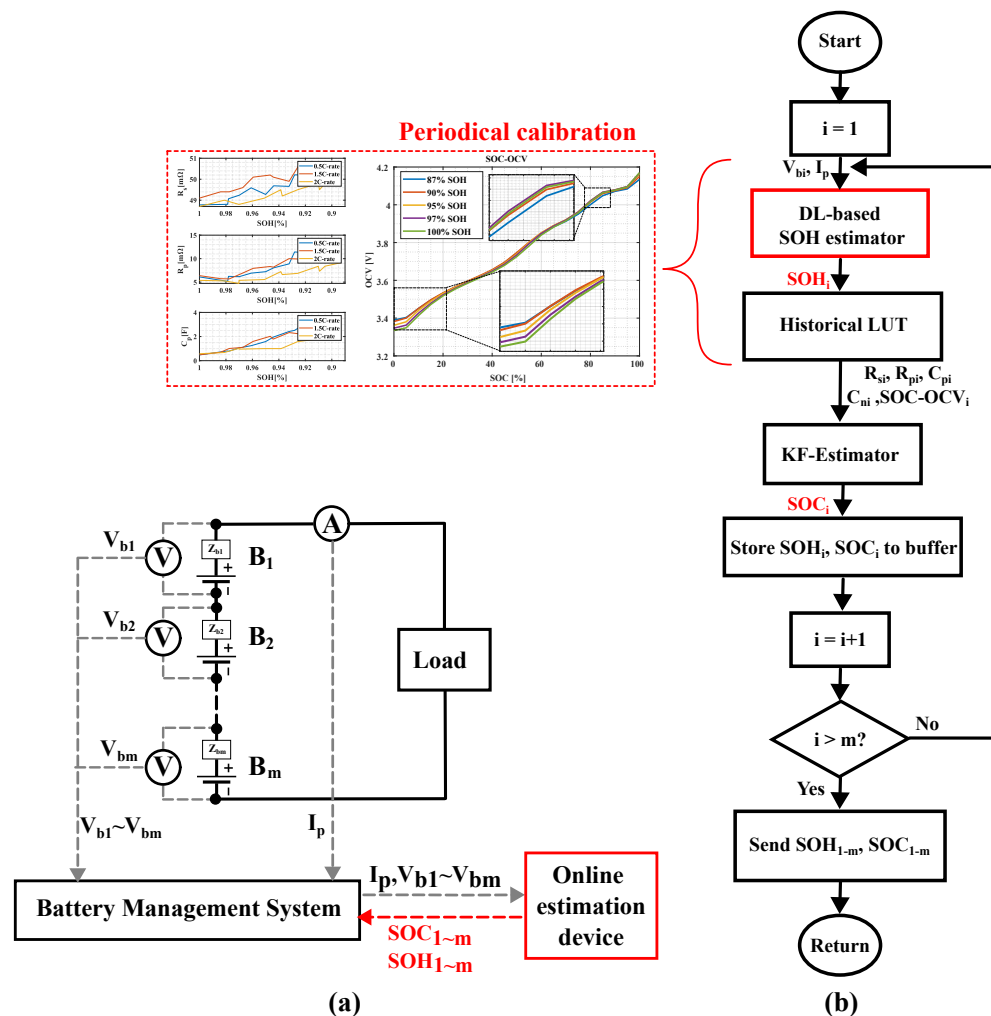


Figure 6. Proposed method: (a) hardware configuration; (b) flowchart.

3.2. Implementation of DL-Based SOH Estimation

Various DL-based approaches can be considered for SOH estimation [28,41,42]. In [43], three different models, including feedforward neural networks (FNNs), convolutional neural networks (CNNs), and long short-term memory (LSTM), were proposed for battery capacity estimation, achieving improved accuracy. FNN has simple architectures that map input features directly to SOH values, whereas CNN has been adapted for sequential data, enabling them to capture spatial dependencies through convolutional layers. Furthermore, LSTM is well suited for SOH estimation due to its ability to model long-term dependencies in time-series data, such as battery charge and discharge cycles. In [41], Transformer models are shown as potential candidates for SOH estimation because they utilize the attention mechanisms to find global dependencies between the input and output using encoder-decoder architectures. Overall, these methods offer distinct advantages in learning complex patterns from the time series prediction problems.

In this work, four methods, including LSTM, CNN, FNN, and Transformer, are implemented for battery SOH estimation. The effect of training data size is also analyzed to choose the suitable model for the DL-based SOH estimator block in Figure 6b. In order to ensure a fair comparison, the NASA B0018 dataset [44] is adopted to evaluate the performance of the SOH estimation methods. In this dataset, the 18,650 lithium-ion battery is charged, discharged, and rested at room temperature. Batteries are charged using the CC-CV method, which applies a constant current of 1.5 A until the voltage reaches the cell voltage limit of 4.2 V, then a constant voltage is employed until the current drops to 20 mA.

The discharge process uses a constant current of 2 A until the cell voltage decreases to 2.5 V. The experimental data are collected until the batteries lose 30% of their rated capacity.

Figure 7 shows the DL model selection process. There are three main steps for this process: data preparation, model training, and performance comparison. In the data preparation stage, battery data are processed to extract battery information with degradation characteristics per cycle. The model is trained by the four model inputs consisting of the current, voltage, temperature, and time together with SOH, which is the reference model output. The cell current and voltage are the primary electrical parameters, which directly reflect the dynamic response of the battery during the charging and discharging process over time, while temperature is a factor that significantly influences the battery performance and aging. These parameters are considered the input features for the DL models due to their relevance in capturing the operational behavior and battery aging. Then, the training data are normalized using the min-max scaler to ensure all features are on a comparable scale, making the training process more effective. Since SOH estimation is a kind of time series prediction problem, a sliding window technique shown in Figure 7a is employed to take advantage of the time dependencies in the data. After that, the data are split into three groups: training, validation, and test sets. While the training set is used for training the model, the validation set is used to protect a model from overfitting or underfitting issues. As seen in Figure 7b, the processed data are used to train four different DL structures during the training stage. After the training processes are completed, the test set is used to obtain the estimation result. After comparing the performance of four DL models, the suitable model is selected.

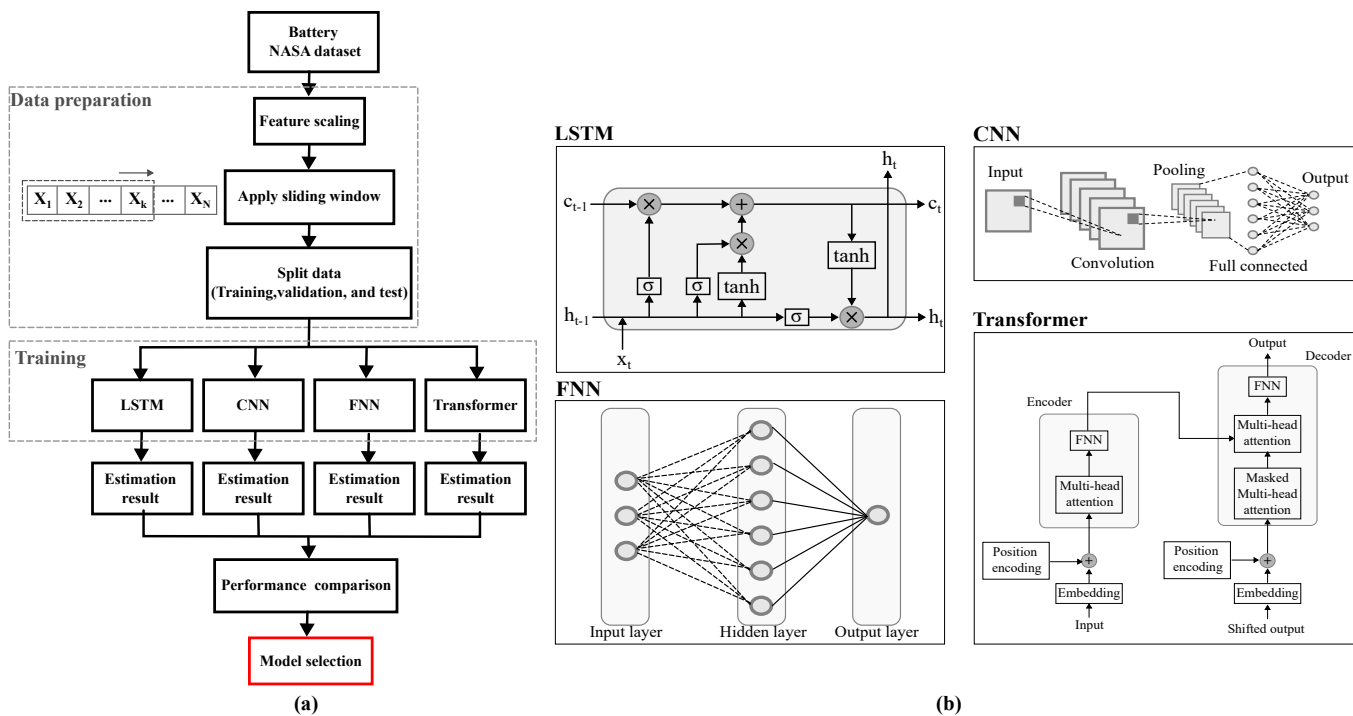


Figure 7. DL model selection process: (a) functional block diagram; (b) implemented DL model architecture.

Each learning method is implemented by Tensorflow 2.17.0 in Python [45] on the AMD Ryzen Threadripper PRO 3955WX 16-Cores of 3.90 GHz and 256 GB memory. Consistent epochs and batch size are used across all models, with 200 epochs and a batch size of 32 to ensure an equitable evaluation. While LSTM is composed of two LSTM layers, each containing 50 hidden units and a fully connected layer for the output, the FNN architecture has a hidden layer with 10 neurons. The Stochastic Gradient Descent (SGD)

optimizer, early stopping, and learning rate reduction are used for both LSTM and FNN. CNN consists of two convolutional layers, each with 64 filters and a kernel size of 3×3 , followed by a fully connected layer. The Adam optimizer is adopted for this case. The Transformer model contains a multi-head attention block with four heads and an FNN with 128 units. The attention mechanism allows the model to capture both short- and long-term dependencies across the sequence. After the attention block, the model passes through a flattening layer and a fully connected layer. The Adam optimizer is also used for the Transformer model.

The Root Mean Squared Error (RMSE) metric is used to evaluate the accuracy of each model, as it gives a relatively high weight to large errors. The RMSE for each DL model is calculated as follows:

$$RMSE = \sqrt{\frac{1}{n} \sum_{i=1}^n (SOH_i - \widehat{SOH}_i)^2}, \quad (17)$$

where SOH_i is the actual value and \widehat{SOH}_i is the predicted value; n is the number of data.

Figure 8 presents a comparison of SOH estimation results of the DL models. Table 1 summarizes the performance for each model across different training data sizes (80%, 60%, and 40%). With 80% of the data used for training, the error across methods is relatively similar; Transformer, LSTM, and FNN perform similarly, while CNN shows slightly higher RMSE. However, when the amount of training data is reduced, the performance difference becomes more noticeable. The CNN model experiences a significant increase in error, with RMSE exceeding 3% for 60% training data and 6% for 40%. In contrast, the Transformer model consistently achieves RMSE below 1%, even with only 40% of the training data, making it the most accurate model overall. The LSTM model also performed well but showed moderate error increases, with an RMSE of 1.87% at 40% training data. The FNN model, despite its simplicity and minimal resource requirements, maintained reasonable accuracy but is lower than Transformer and LSTM, particularly at low training data size.

The comparison highlights key differences in model performance and resource efficiency. The Transformer model shows the highest accuracy, achieving the lowest RMSE values across training data sizes. Because of its attention mechanism, it can effectively capture time dependencies in the data. The LSTM model accuracy also shows high accuracy, but, its performance compared to Transformer is degraded as the training data are reduced. In terms of resource efficiency, the FNN requires the least storage size and the number of parameters, making it a lightweight option. However, its lower accuracy limits its suitability for high-precision SOH estimation. The Transformer model requires more parameters and storage requirements than FNN and LSTM, but less resources than CNN.

To conclude, the FNN model is a lightweight and computationally efficient option for SOH estimation, but lower in accuracy compared to Transformer and LSTM models. The CNN model has the highest number of parameters and storage requirements, but it struggles with reducing training data. Considering the requirements of SOH estimation, both LSTM and Transformer models are suitable due to their ability to handle temporal dependencies. However, the Transformer model can capture long-range dependencies with high accuracy, allowing it to become the preferred choice for applications requiring periodic recalibration of SOH. On the other hand, the SOH model does not require frequent updates, and the longer training time of the Transformer is not a critical issue. Consequently, the Transformer is employed in the proposed periodic SOH estimation.

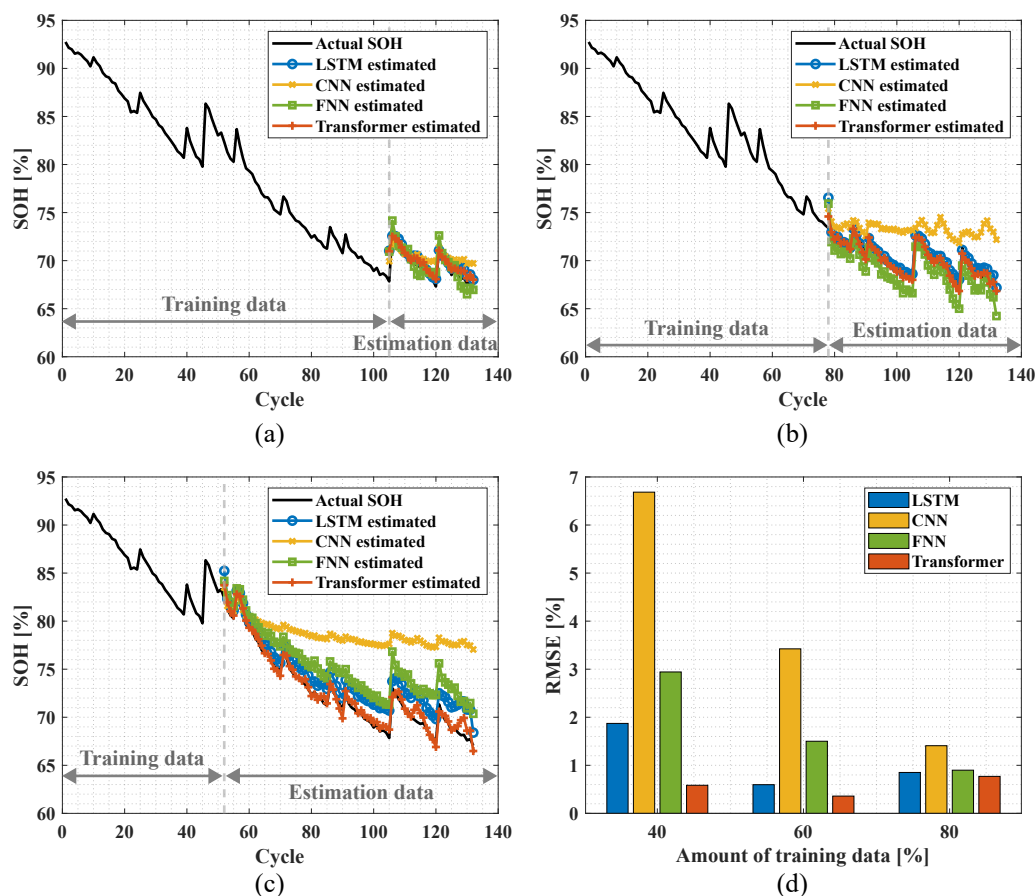


Figure 8. Comparison of SOH estimation from DL models across different training data sizes: (a) 80% dataset; (b) 60% dataset; (c) 40% dataset; (d) RMSE at different training data sizes.

Table 1. DL model comparison.

Method	Performance				
	Parameters	Storage Size [KB]	RMSE ₈₀ [%]	RMSE ₆₀ [%]	RMSE ₄₀ [%]
LSTM	11,053	64	0.85	0.60	1.87
CNN	289,457	1170	1.41	3.42	6.68
FNN	353	21	0.90	1.50	2.94
Transformer	36,425	206	0.77	0.36	0.58

3.3. Implementation of Historical Parameter Lookup Table

Based on the SOH estimation result, a historical parameters look-up table (LUT) is constructed, as shown in Figure 9. This LUT incorporates key parameters that evolve with battery aging, including EIS-model parameters, actual available capacity, and the SOC-OCV relationship. These parameters from the aging dataset are used to dynamically update the state-space model, ensuring it reflects the current SOH. This updated model is implemented into the KF estimator, enhancing the accuracy of SOC estimation. By periodically adapting to the battery's changing characteristics, the proposed approach improves the accuracy of SOC predictions over battery degradation.

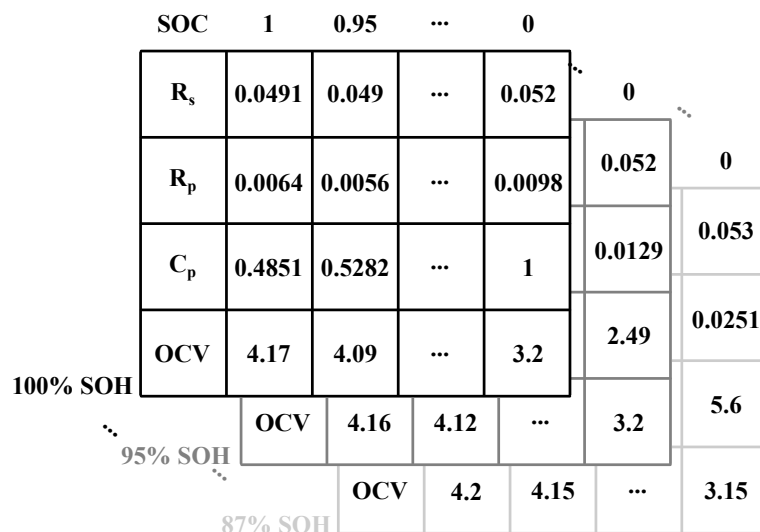


Figure 9. Historical parameter LUT.

4. Performance Verification

4.1. SOH Estimation Performance

At first, the Transformer model-based SOH estimator is applied to the 18,650 cell (Samsung INR, 3.6 V/2.9 Ah). As shown in Figure 10, the model achieves an RMSE of 0.265%, demonstrating its capability to provide accurate SOH predictions.

Next, the model is also applied to a four-cell battery string consisting of cells with different aging states. The SOH estimation results along with their corresponding errors are summarized in Table 2. The Transformer model estimates the SOH with minimal errors within 1% for the first three cells. However, for Cell #4, which exhibits the lowest actual SOH, the model shows a slightly higher error of 1.327%.

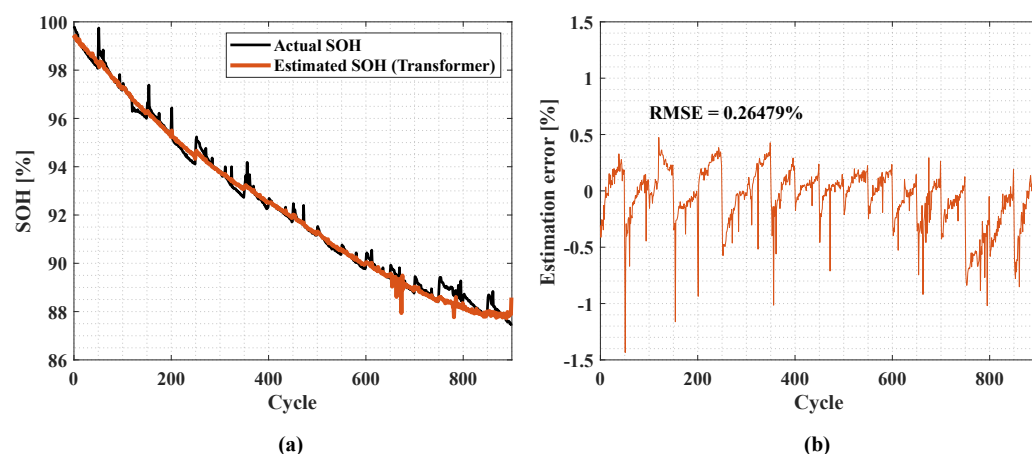


Figure 10. SOH estimation for INR18,650 3.6 V/2.9 Ah cell: (a) SOH estimation using Transformer model; (b) SOH estimation error.

Table 2. SOH estimation for four-series-connected battery string.

Cell	Actual SOH [%]	Estimated SOH [%]	Error [%]
Cell #1	95.13	94.63	-0.526
Cell #2	92.47	92.02	-0.487
Cell #3	89.38	89.53	0.168
Cell #4	87.42	88.58	1.327

4.2. SOC Estimation Performance

The DL-based SOH estimation result in Table 2 is used to update the EKF parameters, including battery EIS-model, OCV-SOC relationships, and actual full capacity, through the historical LUT mentioned in Section 3.3. These updated parameters account for aging effects, significantly improving SOC estimation accuracy.

The EKF-based SOC estimation results are shown in Figure 11 with and without the proposed online calibration algorithm. The test is conducted with 0.5 C-rate charging and 1.5 C-rate discharging for four cells. The results for each cell can be explained as follows.

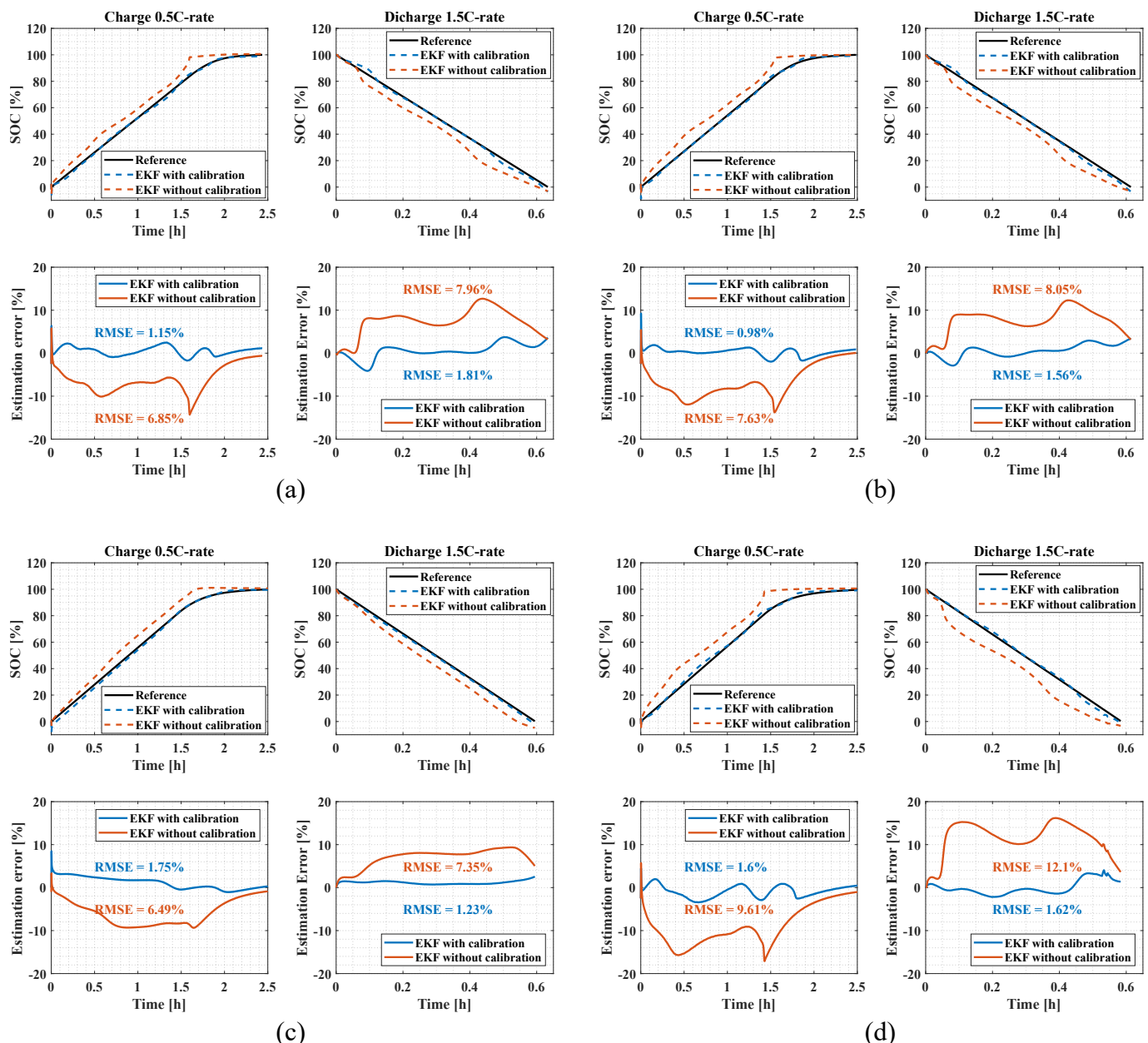


Figure 11. SOC estimation using EKF: (a) cell #1 at 95.13% SOH; (b) cell #2 at 92.47% SOH; (c) cell #3 at 89.38% SOH; (d) cell #4 at 87.42% SOH.

In Figure 11a, the result of cell #1 at 95.13% SOH shows significant estimation errors before incorporating aging adjustments, with RMSE values reaching 6.85% during charging and 7.96% during discharging. The reason comes from the uncalibrated model, which does not consider cell-specific aging characteristics. After applying the proposed online calibration, the RMSE is reduced to 1.15% during charging and below 1.81% overall. For cell

#2 (Figure 11b) at 92.47% SOH, the SOC estimation accuracy becomes poor due to aging effects, showing RMSE values of 7.63% during charging and 8.05% during discharging. However, with the calibration algorithm, the RMSE drops significantly to 0.98% during charging and below 1.56% overall.

In Figure 11c at 89.38% SOH, without adjustments for aging, the RMSE values are 6.49% during charging and 7.35% during discharging, indicating the inaccuracies in SOC estimation of cell #3. These errors are reduced to 1.23% during charging and below 1.75% overall after calibration. Among the tested cells, cell #4 (Figure 11d) exhibits the highest RMSE values due to severe aging effects, reaching 9.61% during charging and 12.1% during discharging at 87.42% SOH. After applying the online calibration algorithm, these errors are significantly reduced to 1.6% and 1.62% during charging and discharging, respectively. These improvements highlight the adaptability of the proposed method in updating the state-space model to reflect current cell characteristics.

These results confirm that the online calibration effectively enhances the accuracy of the SOC estimation for individual cells. Additionally, capacity utilization can be improved since not only the whole SOC of the battery pack but also the individual SOC of the cells can now be monitored. The experimental results have verified the possibility that a low-cost GPU device can successfully perform the entire process at the cell level.

5. Conclusions

This study presents an accurate online calibration method for cell-by-cell SOC estimation. By incorporating online periodic updates of EKF state-space models based on real-time SOH predictions, the method effectively reflects the impact of battery aging. It is also found that the Transformer model is the most suitable for SOH estimation among various DL-based algorithms due to its ability to capture long-term dependencies even with limited data. Even though the validation is experimentally confirmed with four cells, the proposed calibration framework can be applied to any KF-based estimator with a slight modification, providing enhanced accuracy with a lightweight computation device.

Author Contributions: Conceptualization, N.-T.P. and P.-H.L.; data curation, N.-T.P.; funding acquisition, S.-J.C.; investigation, N.-T.P. and P.-H.L.; methodology, N.-T.P., P.-H.L., S.K. and S.-J.C.; project administration, S.-J.C.; resources, S.-J.C.; supervision, S.-J.C.; validation, N.-T.P., P.-H.L., S.K. and S.-J.C.; visualization, N.-T.P., P.-H.L. and S.K.; writing—original draft, N.-T.P. and P.-H.L.; writing—review and editing, S.-J.C. and S.K. All authors have read and agreed to the published version of the manuscript.

Funding: This work was supported by Regional Innovation Strategy (RIS) through the National Research Foundation of Korea (NRF) funded by the Ministry of Education (MOE) (2021RIS-003) and in part by the NRF through the Ministry of Science and ICT(MSICT) under Grant RS-2023-00240194.

Data Availability Statement: The original contributions presented in the study are included in the article, further inquiries can be directed to the corresponding author.

Conflicts of Interest: The authors declare no conflicts of interest.

References

1. European Commission. *A Roadmap for Moving to a Competitive Low Carbon Economy in 2050*; COM (2011)112 final; European Commission: Brussels, Belgium, 2011.
2. International Energy Agency. Global EV Outlook 2024. 2024. Available online: <https://www.iea.org/reports/global-ev-outlook-2024> (accessed on 1 December 2024).
3. BloombergNEF. Lithium-Ion Battery Pack Prices Hit Record Low of \$139/kWh. *BloombergNEF*, 26 November 2023.

4. See, K.W.; Wang, G.; Zhang, Y.; Wang, Y.; Meng, L.; Gu, X.; Zhang, N.; Lim, K.C.; Zhao, L.; Xie, B. Critical review and functional safety of a battery management system for large-scale lithium-ion battery pack technologies. *Int. J. Coal Sci. Technol.* **2022**, *9*, 36. [[CrossRef](#)]
5. Lu, L.; Han, X.; Li, J.; Hua, J.; Ouyang, M. A review on the key issues for lithium-ion battery management in electric vehicles. *J. Power Sources* **2013**, *226*, 272–288. [[CrossRef](#)]
6. Lipu, M.S.H.; Mamun, A.A.; Ansari, S.; Miah, M.S.; Hasan, K.; Meraj, S.T.; Abdolrasol, M.G.; Rahman, T.; Maruf, M.H.; Sarker, M.R.; et al. Battery Management, Key Technologies, Methods, Issues, and Future Trends of Electric Vehicles: A Pathway toward Achieving Sustainable Development Goals. *Batteries* **2022**, *8*, 119. [[CrossRef](#)]
7. La, P.H.; Nguyen, N.A.; Choi, S.J. Average Model of Switched-Energy-Tank Battery Equalizer for Accelerated Performance Assessment. *Energies* **2024**, *17*, 631. [[CrossRef](#)]
8. Girijaprasanna, T.; Dhananjayulu, C. A Review on Different State of Battery Charge Estimation Techniques and Management Systems for EV Applications. *Electronics* **2022**, *11*, 1795. [[CrossRef](#)]
9. Hansen, T.; Wang, C.J. Support vector based battery state of charge estimator. *J. Power Sources* **2005**, *141*, 351–358. [[CrossRef](#)]
10. Rivera-Barrera, J.P.; Muñoz-Galeano, N.; Sarmiento-Maldonado, H.O. SoC Estimation for Lithium-ion Batteries: Review and Future Challenges. *Electronics* **2017**, *6*, 102. [[CrossRef](#)]
11. Kim, J.; Cho, B. Screening process-based modeling of the multi-cell battery string in series and parallel connections for high accuracy state-of-charge estimation. *Energy* **2013**, *57*, 581–599. [[CrossRef](#)]
12. Zhang, C.; Jiang, Y.; Jiang, J.; Cheng, G.; Diao, W.; Zhang, W. Study on battery pack consistency evolutions and equilibrium diagnosis for serial-connected lithium-ion batteries. *Appl. Energy* **2017**, *207*, 510–519. [[CrossRef](#)]
13. Schuster, S.F.; Bach, T.; Fleder, E.; Müller, J.; Brand, M.; Sextl, G.; Jossen, A. Nonlinear aging characteristics of lithium-ion cells under different operational conditions. *J. Energy Storage* **2015**, *1*, 44–53. [[CrossRef](#)]
14. Gong, X.; Xiong, R.; Mi, C.C. Study of the characteristics of battery packs in electric vehicles with parallel-connected lithium-ion battery cells. *IEEE Trans. Ind. Appl.* **2014**, *51*, 1872–1879. [[CrossRef](#)]
15. Zheng, Y.; Ouyang, M.; Lu, L.; Li, J. Understanding aging mechanisms in lithium-ion battery packs: From cell capacity loss to pack capacity evolution. *J. Power Sources* **2015**, *278*, 287–295. [[CrossRef](#)]
16. Park, S.; Ahn, J.; Kang, T.; Park, S.; Kim, Y.; Cho, I.; Kim, J. Review of state-of-the-art battery state estimation technologies for battery management systems of stationary energy storage systems. *J. Power Electron.* **2020**, *20*, 1526–1540. [[CrossRef](#)]
17. Zhang, Z.; Jiang, L.; Zhang, L.; Huang, C. State-of-charge estimation of lithium-ion battery pack by using an adaptive extended Kalman filter for electric vehicles. *J. Energy Storage* **2021**, *37*, 102457. [[CrossRef](#)]
18. Ng, K.S.; Moo, C.S.; Chen, Y.P.; Hsieh, Y.C. Enhanced coulomb counting method for estimating state-of-charge and state-of-health of lithium-ion batteries. *Appl. Energy* **2009**, *86*, 1506–1511. [[CrossRef](#)]
19. Zhao, L.; Lin, M.; Chen, Y. Least-squares based coulomb counting method and its application for state-of-charge (SOC) estimation in electric vehicles. *Int. J. Energy Res.* **2016**, *40*, 1389–1399. [[CrossRef](#)]
20. Plett, G.L. Extended Kalman filtering for battery management systems of LiPB-based HEV battery packs: Part 3. State and parameter estimation. *J. Power Sources* **2004**, *134*, 277–292. [[CrossRef](#)]
21. Pulavarthi, C.; Kalpana, R.; Parthiban, P. State of Charge estimation in Lithium-Ion Battery using model based method in conjunction with Extended and Unscented Kalman Filter. In Proceedings of the 2020 International Conference on Power Electronics and Renewable Energy Applications (PEREA), Kannur, India, 27–28 November 2020; IEEE: Piscataway, NJ, USA, 2020; pp. 1–6.
22. Jokić, I.; Zečević, Ž.; Krstajić, B. State-of-charge estimation of lithium-ion batteries using extended Kalman filter and unscented Kalman filter. In Proceedings of the 2018 23rd International Scientific-Professional Conference on Information Technology (IT), Zabljak, Montenegro, 19–24 February 2018; IEEE: Piscataway, NJ, USA, 2018; pp. 1–4.
23. Khanum, F.; Louback, E.; Duperly, F.; Jenkins, C.; Kollmeyer, P.J.; Emadi, A. A Kalman filter based battery state of charge estimation MATLAB function. In Proceedings of the 2021 IEEE Transportation Electrification Conference & Expo (ITEC), Chicago, IL, USA, 21–25 June 2021; IEEE: Piscataway, NJ, USA, 2021; pp. 484–489.
24. Chu, Y.; Li, J.; Gu, J.; Qiang, Y. Parameter identification and SOC estimation of lithium-ion batteries based on AGCOA-ASRCKF. *J. Power Electron.* **2023**, *23*, 308–319. [[CrossRef](#)]
25. Rothenberg, T. *State Space Models and the Kalman Filter*; University of California: Oakland, CA, USA, 2007. Available online: <https://eml.berkeley.edu/~rothenbe/Fall2007/kalman.pdf> (accessed on 20 June 2022).
26. QuantStart. State Space Models and the Kalman Filter. Available online: <https://www.quantstart.com/articles/State-Space-Models-and-the-Kalman-Filter/> (accessed on 23 June 2022).
27. Shen, W.; Chan, C.; Lo, E.; Chau, K. A new battery available capacity indicator for electric vehicles using neural network. *Energy Convers. Manag.* **2002**, *43*, 817–826. [[CrossRef](#)]
28. Salkind, A.J.; Fennie, C.; Singh, P.; Atwater, T.; Reisner, D.E. Determination of state-of-charge and state-of-health of batteries by fuzzy logic methodology. *J. Power Sources* **1999**, *80*, 293–300. [[CrossRef](#)]

29. Vidal, C.; Malysz, P.; Kollmeyer, P.; Emadi, A. Machine learning applied to electrified vehicle battery state of charge and state of health estimation: State-of-the-art. *IEEE Access* **2020**, *8*, 52796–52814. [[CrossRef](#)]
30. Yao, F.; Meng, D.; Wu, Y.; Wan, Y.; Ding, F. Online health estimation strategy with transfer learning for operating lithium-ion batteries. *J. Power Electron.* **2023**, *23*, 993–1003. [[CrossRef](#)]
31. Huang, S.; Li, J.; Wu, L.; Zhang, W. Data quality augmentation and parallel network modeling for residual life prediction of lithium-ion batteries. *J. Power Electron.* **2024**, *24*, 955–963. [[CrossRef](#)]
32. Cui, Z.; Dai, J.; Sun, J.; Li, D.; Wang, L.; Wang, K. Hybrid methods using neural network and Kalman filter for the state of charge estimation of lithium-ion battery. *Math. Probl. Eng.* **2022**, *2022*, 9616124. [[CrossRef](#)]
33. Shu, X.; Li, G.; Zhang, Y.; Shen, S.; Chen, Z.; Liu, Y. Stage of charge estimation of lithium-ion battery packs based on improved cubature Kalman filter with long short-term memory model. *IEEE Trans. Transp. Electrif.* **2020**, *7*, 1271–1284. [[CrossRef](#)]
34. Yu, Z.; Liu, J.; Lu, Y.; Feng, C.; Li, L.; Wu, Q. Combined EKF-LSTM algorithm-based enhanced state-of-charge estimation for energy storage container cells. *J. Power Electron.* **2024**, *24*, 1329–1339. [[CrossRef](#)]
35. Kim, M.; Kim, K.; Kim, J.; Yu, J.; Han, S. State of charge estimation for lithium Ion battery based on reinforcement learning. *IFAC-PapersOnLine* **2018**, *51*, 404–408. [[CrossRef](#)]
36. Li, M.; Zhang, Y.; Hu, Z.; Zhang, Y.; Zhang, J. A battery SOC estimation method based on AFFRLS-EKF. *Sensors* **2021**, *21*, 5698. [[CrossRef](#)] [[PubMed](#)]
37. Jiani, D.; Zhitao, L.; Can, C.; Youyi, W. Li-ion battery SOC estimation using EKF based on a model proposed by extreme learning machine. In Proceedings of the 2012 7th IEEE Conference on Industrial Electronics and Applications (ICIEA), Singapore, 18–20 July 2012; IEEE: Piscataway, NJ, USA, 2012; pp. 1651–1656.
38. Sharifi-Asl, S.; Taylor, M.L.; Lu, Z.; Engelhardt, G.R.; Kursten, B.; Macdonald, D.D. Modeling of the electrochemical impedance spectroscopic behavior of passive iron using a genetic algorithm approach. *Electrochim. Acta* **2013**, *102*, 161–173. [[CrossRef](#)]
39. Seaman, A.; Dao, T.S.; McPhee, J. A survey of mathematics-based equivalent-circuit and electrochemical battery models for hybrid and electric vehicle simulation. *J. Power Sources* **2014**, *256*, 410–423. [[CrossRef](#)]
40. Chui, C.K.; Chen, G. Extended Kalman filter and system identification. In *Kalman Filtering*; Springer: Berlin/Heidelberg, Germany, 2017; pp. 115–137.
41. Süzen, A.A.; Duman, B.; Şen, B. Benchmark analysis of jetson tx2, jetson nano and raspberry pi using deep-cnn. In Proceedings of the 2020 International Congress on Human-Computer Interaction, Optimization and Robotic Applications (HORA), Ankara, Turkey, 26–27 June 2020; IEEE: Piscataway, NJ, USA, 2020; pp. 1–5.
42. Guirguis, J.; Ahmed, R. Transformer-Based Deep Learning Models for State of Charge and State of Health Estimation of Li-Ion Batteries: A Survey Study. *Energies* **2024**, *17*, 3502. [[CrossRef](#)]
43. Oji, T.; Zhou, Y.; Ci, S.; Kang, F.; Chen, X.; Liu, X. Data-driven methods for battery soh estimation: Survey and a critical analysis. *IEEE Access* **2021**, *9*, 126903–126916. [[CrossRef](#)]
44. Choi, Y.; Ryu, S.; Park, K.; Kim, H. Machine learning-based lithium-ion battery capacity estimation exploiting multi-channel charging profiles. *IEEE Access* **2019**, *7*, 75143–75152. [[CrossRef](#)]
45. Saha, B. Battery Data Set. In *NASA AMES Prognostics Data Repository*; NASA Ames Research Center: Moffett Field, CA, USA, 2007.
46. Abadi, M.; Barham, P.; Chen, J.; Chen, Z.; Davis, A.; Dean, J.; Devin, M.; Ghemawat, S.; Irving, G.; Isard, M.; et al. TensorFlow: A system for Large-Scale machine learning. In Proceedings of the 12th USENIX Symposium on Operating Systems Design and Implementation (OSDI 16), Savannah, GA, USA, 2–4 November 2016; pp. 265–283.

Disclaimer/Publisher’s Note: The statements, opinions and data contained in all publications are solely those of the individual author(s) and contributor(s) and not of MDPI and/or the editor(s). MDPI and/or the editor(s) disclaim responsibility for any injury to people or property resulting from any ideas, methods, instructions or products referred to in the content.